CHAPTER 2

DESIGN INVESTIGATIONS AND PIC SIMULATION OF SINGLE FREQUENCY RELATIVISTIC BACKWARD WAVE OSCILLATOR

CONTENTS

*Part of this work has been published as:

V. Venkata Reddy, Mumtaz Ali Ansari and M.Thottappan, "Simulation Investigations of High Power Overmoded Relativistic Backward Wave Oscillator with Trapezoidal Resonant Reflector," ***Defence Science Journal***, vol. 71, no. 3, pp. 346-350, May 2021 (10.14429/dsj.71.16745).

CHAPTER 2: DESIGN INVESTIGATIONS AND PIC SIMULATION OF SINGLE FREQUENCY RELATIVISTIC BACKWARD WAVE OSCILLATOR

2.1 Introduction

The operation of any High-Power Microwave (HPM) sources is understood based on the interaction between the electron beam and electromagnetic (EM) wave induced by an interaction structure, which is called beam-wave interaction. The principle of operation of the RBWO is Cherenkov radiation. In RBWO, the annular electron beam is used such that the dominant slow space charge wave associated with beam is closer to interaction structure surface. SWS's are used for beam-wave interaction. The beam-wave interaction behavior inside the HPM source is understood based on the interaction between the slow or fast space charge waves and the RF wave present in the interaction structure. The slow space charge waves are referred as the waves with the phase velocities slower than the electron beam velocity, conversely the fast space charge waves are referred as the waves with phase velocities faster than the velocity of the beam. The HPM generation requires an external DC magnetic field to retain the electron beam in trajectory. For an efficient operation at higher power levels, it would be desirable to have an oscillator that operates at lower impedance and also eliminate the problem of voltage matching. RBWO is one of the most promising examples of HPM sources, which effectively and efficiently utilize the energy of slow space charge wave associated with high current and voltage version of electron beam called IREB. The HPM sources like relativistic magnetron and MILO can generate RF output power around 5 GW, but suffers from pulse shortening at this level of RF power, even RBWO also [3], but this problem can be overcome to some extent by modifying the reflector and SWS of an RBWO, which helps the device to generate RF output power up to 100

ns. The HPM source Vircator can also generate power in GW range, but the generation efficiency is very less around 3 % [3], [20]. Reltron is another class of HPM source quite similar to RKAs, can generate RF power in 100s of MW range for more than 100 ns with efficiency around 40 % [43], [46]. The first experimental demonstration of an RBWO held at Cornell University [65] since then great advancements and improvements has been done in the era of RBWO development and many more is going on. The main drawback of an RBWO is the requirement of external magnetic field, however an extensive research is going on to reduce the guiding magnetic field requirement in the range of permanent magnets [6], [91]. Generation of RF output power at low guiding magnetic field with high conversion efficiency is a big task to be achieved and required extensive research to be done. J.R. Pierce developed the first linear theory for low power TWTs and BWOs [69, 70], but for high current and voltage versions of conventional devices, the behavior is described by non-linear theories. In non-linear theory, the various effects that were ignored to formulate the linear theory are taken into consideration. G.N. Rapoport developed the non-linear theory corresponds to stationary oscillations in non-relativistic BWOs [71] and later it was extended for ultra-relativistic BWOs by Kovalev *et al*. [72] in 1975. The various theories for relativistic BWOs were developed during earlier stage of 1980s, which helps to develop device working and analytical understanding [73-78]. RBWO can also generate dual-band/ dual-frequency generation with GW power level.

In the present chapter, with the help of typical 2D schematic of an RBWO with reflector, the operating principle of the Relativistic BWO is presented. The brief description and design methodology for each subassembly of the device is defined and presented. The analytical fundamentals of the RBWO, such as, dispersion diagram of SWS (interaction structure), etc. is also formulated for the device and validated through

the published experimental values. The cavity rectangular RR is replaced with Trapezoidal RR to enhances the pre-modulation during electron beam propagation, thus increasing the generated RF signal overall efficiency and coherency. The improved Particle-In-Cell simulation results are also presented. Further, the influence of different design parameters on frequency, RF output power, and efficiency are analyzed through Particle-In-Cell (PIC) simulations.

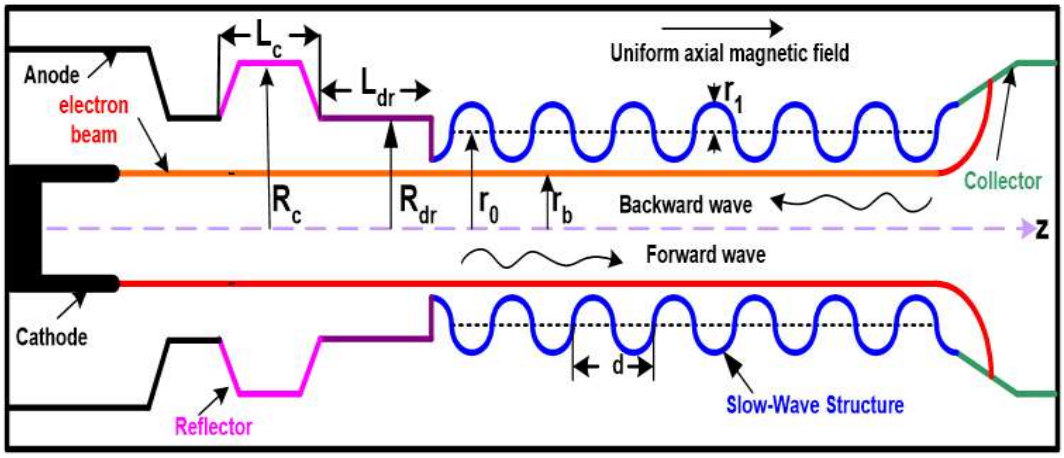

Figure 2.1: Schematic of RBWO with overmoded SWS and TRR.

2.2 Operating Principle and Condition for Sustained Oscillation

The fundamental components of RBWO are relativistic electron beam, SWS, and guiding magnetic field. The external magnetic field guides the IREB through the SWS as shown in Figure 2.1. The strong guiding magnetic field makes the transverse motion of beam negligible such that the electron beam moves only in axial direction but under low magnetic field the azimuthal motion of beam affects the beam-wave interaction between IREB and SWS. The thin annular IREB having radius r_b is emitted by the cathode with EEE, guided by the external guiding magnetic field inside the structure having rippled walls. The SWS reduced the phase velocity of (EM) waves parallel to the axial velocity of electron beam such that the relativistic electron beam can give up energy directly to one of the eigenmodes of the structure. The eigenmodes of the

structure have negative group velocity such that the electron energy will be transferred to RF wave in the opposite direction of electron beam direction, and the device is therefore designated as a backward wave oscillator. RBWO is an O-type Cerenkov radiation-based device which generally required transverse magnetic (TM) modes of operation as it has an axial electric field component. In general, corrugated waveguide also supports hybrid modes such as, HE and EH. In HE modes, the TE (H) wave dominates, while in EH modes TM (E) wave dominates [109]. The TM modes and hybrid modes (HE and EH) have E_z component that perturbs the axial velocity of electron beam and causes an absolute instability.

In general, the basic requirement for the oscillations to be sustained in any oscillator (SSDs or VEDs) is that the total phase shift should be an even integer multiple of π provided that the gain per feedback loop is sufficient. The same concept is applied to understand the oscillating principle of RBWO [110]. Let's considered an electron beam streaming in the forward direction inside the SWS and RF wave propagating in backward direction for a single SWS period of length 'd' providing a total phase shift of θ_1, as shown in Figure 2.2. Similarly, one can assume θ_2 for two SWS period and so on, 'k_0d' is the fundamental phase shift per period of RF wave at the left and 'k_ed' is the

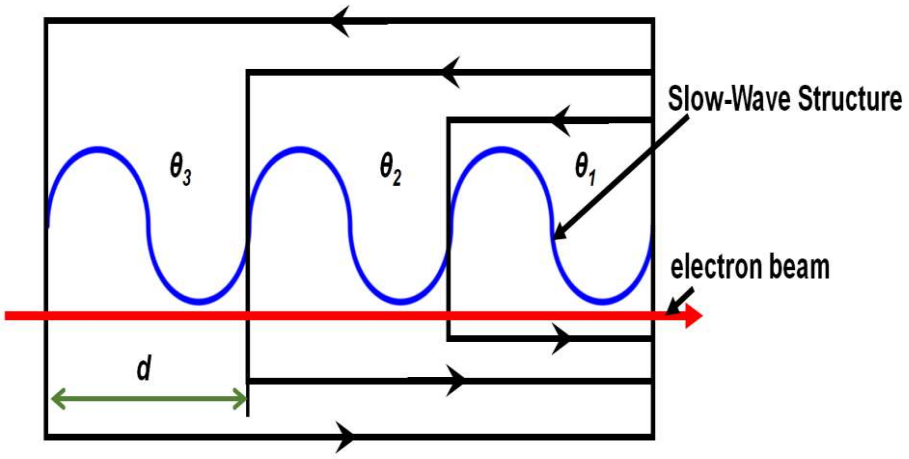

Figure 2.2: Working principle for sustained oscillation.

phase shift in the RF wave, which occurs when the beam travels the distance of '*d*'. The fundamental phase shift in -1st space harmonic of RF wave at the operating frequency is '$k_{-1}d$' for a one period. Thus

$$\theta_1 = 1(k_e d + k_o d) \quad \text{----- one period}$$

$$\theta_2 = 2(k_e d + k_o d) \quad \text{----- two periods}$$

$$\theta_3 = 3(k_e d + k_o d) \quad \text{----- three periods}$$

$$\vdots$$

$$\vdots$$

$$\theta_N = N(k_e d + k_o d) \quad \text{----- N periods} \qquad (2.1)$$

From Figure 2.3, the relation between $k_{-1}d$ and k_0d are

$$k_{-1}d = 2\pi - k_o d \qquad (2.2)$$

and, the equation of (2.2) must be equal to $k_e d$ under the condition of synchronism i.e., $k_e d = k_{-1}d$.

$$\therefore k_e d = 2\pi - k_o d \qquad (2.3)$$

substituting equation (2.3) in (2.1), we get

$$\theta_1 = 2\pi \text{ ----- one period}$$

$$\theta_2 = 4\pi \text{ ----- two periods}$$

$$\theta_3 = 6\pi \text{ ----- three periods}$$

$$\vdots$$

$$\vdots$$

$$\theta_N = 2N\pi \text{ ----- N periods} \qquad (2.4)$$

Thus, the total phase shift for each feedback loop is an integral multiple of 2π radians. Hence, the tube will oscillate provided that the total loop gain must be sufficient. If the

gain is not sufficient for oscillation, the tube will act as a narrow band regenerative amplifier. For an oscillator, they do not require an input signal, however the oscillations are generated by an infinitesimal noise signal at the desired operating frequency build-up due to feedback (positive) until a stable operating point is reached. The operation of the RBWO proceeds as: The beam current is increased from zero by increasing the radial gap between anode and cathode with a constant beam voltage. As the beam current increases, the gain for feedback loop increases. Finally, a point is reached where the interaction structure breaks into oscillation. The dc beam current at this point is termed the starting current, I_{st}. Finally, the interaction structure reaches a point where it breaks down into oscillations. At this point the dc beam current is called the starting current, I_{st}.

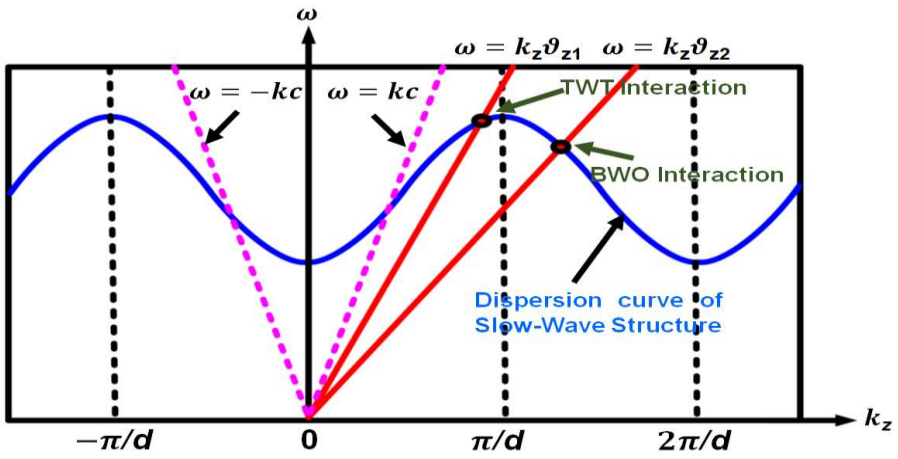

Figure 2.3: The Brillouin diagram of the slow-Wave Structure.

2.3 Modeling of Sub-Assemblies

The relativistic BWOs mainly consist of an annular cathode, reflector, drift section, slow-wave structure, tapered collector, and external guiding magnetic field as shown in Figure 2.1.

2.3.1 Annular Cathode

In HPM devices, the cathode generally used for the generation of the relativistic electron beam is called cold cathode (explosive emission cathode) and the basic physics for electron emission is EEE. Explosive emission cathode is used for GW class of HPM sources because such cathodes get "turn-on" at relatively low electric fields and deliver very high-current densities of 100's of A /cm^2 that allows the tube to generate extremely high RF power. In short, the occurrence of high DC voltages causes electrons to escape from the cathode surface due to the induction of a very high electric field. Graphite/Caesium Iodide (CsI) coated or velvet is used as an explosive emission point to achieve a high EEE [3]. Graphite is generally used because it has a lower electric breakdown strength (175 kV/cm) as compared to Stainless Steel (300 kV/cm), Aluminum (290 kV/cm) and Molybdenum (460 kV/cm). Beside this Graphite has maximum melting point among all-around 43000 K and also the electron emission is copious. In RBWO, an annular electron beam is used such that the dominant slow space charge wave associated with beam is closer to SWS surface and also the space charge limiting current of the device is enhanced. The radius of explosive emission annular cathode (r_b) is calculated such that it will interact with maximum electric field of operating mode only. The intensity of cyclotron suppression for the operating modes (for all TE and TM modes except TM_{01}) and for the beam to mean radius ratio has to be zero for no cyclotron absorption, *i.e.* [111]

$$J_{m\pm1}^2\left(\frac{\chi_{mn} r_b}{r_o}\right) = 0 \qquad (2.5)$$

where, r_0 is the mean radius of SWS, m is full sine variation in azimuthal direction and n is half-sine variation in radial direction in cylindrical coordinate. By solving (2.5), the

beam radius is calculated around $r_b \approx 0.7 r_0$. The calculated value is independent of beam parameters and operating frequency.

2.3.2 Reflector

In the beginning of the RBWO era, the RF output power was collected from the cathode end of the interaction structure. Later, to extract the generated RF power axially at the output tapered collector, researchers started using a reflector at the upstream section of RBWO near to the cathode. The backward propagating TM_{0n} mode is reflected to forward propagating TM_{0n} mode by the reflector. The beam does not interact with the forward wave but there is a chance that the forward wave gets reflected at the end of SWS because of poor coupling with the tapered collector or output horn. There are many types of reflectors such as cut-off neck reflector, cavity resonant reflector (RR) and Bragg reflector.

2.3.2.1 Cut-off Neck Reflector

It is simply a cylindrical section having radius R_{cut} and length L_{cut} as shown in Figure 2.4. The radius of the reflector is calculated in such a way that it should have a cut-off frequency more than the operating frequency of backward propagating wave such that the backward propagating mode become forward propagating mode and is given by [3], [112]

$$R_{cut} \approx \frac{\chi_{mn} c}{2\pi f_c} \tag{2.6}$$

where, χ_{mn} is the Eigen value of operating mode to be cut-off, c is the speed of light and f_c is the cut-off frequency, which is more than the operating frequency. The cut-off reflector has got an advantage that it can reflect any mode whether TM_{mn} or TE_{mn}. Beside this advantage, it has many disadvantages such as limitation to beam wall

distance, weak beam-wave coupling and plasma formation at the neck section. These disadvantages restrict the RBWO device to generate short pulse (less than 30 ns) with power conversion efficiency very less than 30 %.

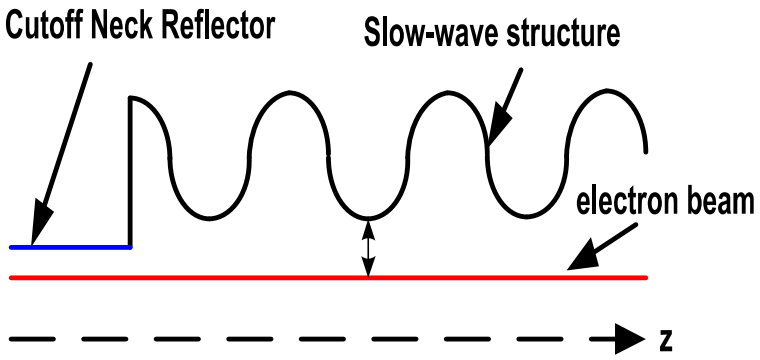

Figure 2.4: Schematic of cut-off neck reflector.

2.3.2.2 Cavity Resonant Reflector (RR) with Drift Section

The second reflector is cavity resonant reflector (RR) having an axis-symmetric groove of radius r_c and length L_c present at the upstream section of the device near to cathode. It is an open cavity-type reflector followed by a drift waveguide having radius r_{dr} and length of about L_{dr}, as shown in Figure 2.5. The restriction on these dimensions for the existence of at least one trapped mode oscillation of TM_{02} is [113],

$$\frac{\chi_{02}}{r_c} < \frac{\omega}{c} < \frac{\chi_{02}}{r_{dr}} \tag{2.7}$$

and

$$\chi_{02} \times L_c \sqrt{1 - r_{dr}^2 / r_c^2} < 2 \times r_{dr} \tag{2.8}$$

where, χ_{02} is Eigen value of TM_{02} mode. The length of the waveguide is very important as it decides the depth of velocity modulation and also at the same time it determines the phase difference between the modulating field and space harmonics of

wave at the starting of SWS [6]. Further, according to mode matching method, the RR parameters can be calculated by [113]

$$\tan\left(\sqrt{(\omega/c)^2-(\chi_{02}/r_c)^2}\times\frac{L_c}{2}\right)=\frac{\sqrt{(\omega/c)^2-(\chi_{02}/r_c)^2}}{\sqrt{(\chi_{02}/r_{dr})^2-(\omega/c)^2}} \tag{2.9}$$

where, ω is angular resonant frequency and c is the speed of light. The radius and length of drift section are chosen such that it should favor the interaction of desired mode only and does not allow the propagation of TM_{02} mode at the same operating frequency. The radius and length of RR can also be calculated directly as,

$$r_c \approx \frac{\chi_{mn}c}{2\pi f_r} \tag{2.10}$$

and

$$L_c \le \frac{\lambda_r}{3} \tag{2.11}$$

where, f_r and λ_r is the resonating frequency and wavelength, respectively. The radius of the cavity RR and drift section is restricted by

$$\frac{\chi_{mn}}{r_c} < k < \frac{\chi_{mn}}{r_{dr}} \tag{2.12}$$

where, $k = 2\pi/\lambda_r$ [114]. The radius and length of drift section are chosen such that it should cut-off TM_{02} mode and can be calculated approximately

$$r_{dr} > \frac{\chi_{mn}c}{2\pi f} \tag{2.13}$$

and

$$0.5\lambda_r < L_{dr} < \lambda_r \tag{2.14}$$

Mechanical tuning is obtained by varying the distance between RR and SWS, as it changes the phase and synchronism condition between slow space charge wave and -1st harmonics of fundamental mode [115]. It is basically due to the preliminary modulation of the beam electrons that also caused the velocity modulation of electrons passing through it leads to electron bunching. One can easily understand that the frequency tuning is achieved by changing or altering the beam energy or velocity or trajectory termed as beam loading by means of magnetic field or voltage or varying L_{dr}. The cavity RR has many advantages over cut-off neck reflector such as it provides pre-bunched electrons to enter the SWS, which enhanced the coherency and generation efficiency of the device, reduce the start current and let the device saturate fast, allow the device to operate at low guiding magnetic field [6], mechanical tuning by shifting it around SWS, minimize the beam-SWS gap closer to improve coupling, and also helps in increasing the pulse width of generated RF power. Besides this, the RR suffers from one disadvantage that it can only reflect the azimuthal symmetric TM modes as these modes have surface current distribution in longitudinal direction only. The cavity RR is transverse to these surface current lines, which make it short circuit to backward propagating TM_{0n} mode.

At the GW power level and as the output power increases, the electric field near to the edge of RR strengthened and caused a breakdown. Due to the increase in the field beyond the threshold value, the electrons emitted from the edge of the RR and accelerated by the axial RF and restricted in transverse direction by the external guiding magnetic field. These electrons get bombarded on the opposite surface of RR near to cathode and microwave generation gets terminated due to the plasma formation inside RR, which shorted the opposite surfaces, the mentioned process is termed as pulse shortening [113]. So, there is a need to modify the cavity RR such that the field gets

redistributed around the reflector. The possible method is to use distributed reflection structure consists of several RR is used and in which each resonant cavity will reflect fraction of backward TM_{01} wave and thus field is get distributed among each cavity. But the main disadvantage of such structure is that the device length will increase and unsuitable resonance matching between RRs and hence losses will increase. Further, the cavity RR can modify into trapezoidal cavity RR, as shown in Figure 2.6 [96].

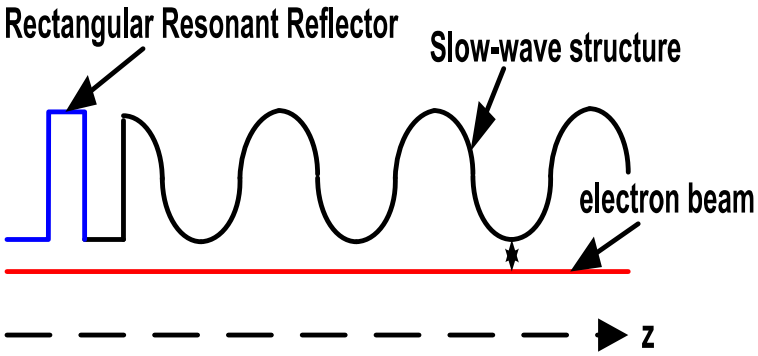

Figure 2.5: Schematic of Cavity RR.

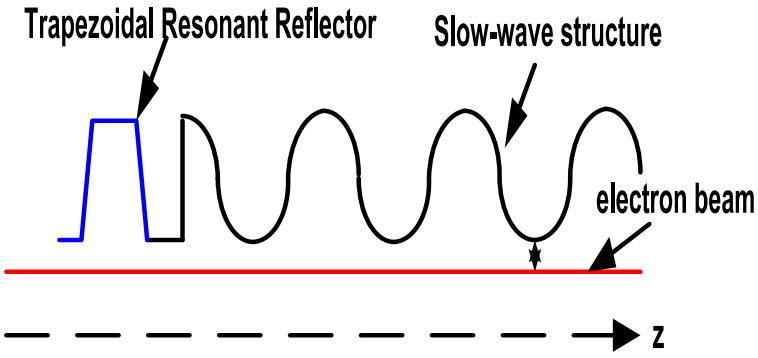

Figure 2.6: Schematic of Trapezoidal RR (TRR).

2.3.2.3 Bragg Reflector

Bragg structure is made up of sinusoidal left and right corrugated waveguide with wall radius varies as [116, 117],

$$R_w = R_0 + \sin(\bar{k}z + m\phi) \tag{2.15}$$

where, R_0 and R_1 are the mean radius and depth of corrugation, respectively, $\bar{k} = 2\pi / p$ where, P is the axial period of Bragg and m is number of fold that can be calculated as, $m = \pm(m_H - m_E)$ (different signs are related to left hand (-) and right hand (+) helical corrugations), where, m_H and m_E are the azimuthal index of transverse electric (TE_{mn}) and transverse magnetic (TM_{mn}) mode, respectively, and ± indicates the directional rotation of polarization. The Bragg structure can play multiple roles like a reflector, a mode converter, and it can also act like as an interaction circuit resonating at some frequency [122]. The main disadvantage of the Bragg structure is that the pulse shortening at a low guiding magnetic field, therefore the device acts as an interaction structure to produce a second frequency in addition to SWS.

2.3.3 Slow Wave Structure (SWS)

The RBWO is devised by considering Cherenkov radiation that is emitted by an electron when it travels with a velocity approximately equal to the speed of light in that particular medium. SWS is the most important section of RBWO generally referred as the heart of the device. Cherenkov radiation was experimentally observed by Cherenkov [118] in 1934, which was explained by Tamm [119] more correctly after three years. However, the Cherenkov radiation is spontaneous in nature while there is a requirement of homogeneous radiation, which can be radiated with the help of bunch of electrons. The SWS causes velocity modulation of traversed electrons, which leads to the bunching of electrons. The generation of EM in such devices depends on two basic conditions such as: (i) the axial electric field must exists to perturb the axially traveling electron beam under the external guiding magnetic field, and (ii) the phase velocity of generated RF must be parallel to the beam velocity termed as Cherenkov resonance condition. SWS is an electrodynamic structure termed as interaction circuit, which

slows down the phase velocity of supported RF eigenmodes to get in synchronism (called Cherenkov synchronism) with the velocity of electron beam for transferring of energy from beam to RF. Numerous RBWOs have been reported with different SWSs such as as iris-loaded waveguide [121], rippled wall waveguide [66], helix [120], sinusoidally corrugated waveguide [74], trapezoidal corrugated waveguide [122], and combination of rectangular and sinusoid [123]. In the present studies, the sinusoidal corrugation is considered because of its smooth wall profile which helps in reducing the localized electric field at the sharped edges. The wall radius cylindrical waveguide depends on azimuthal (ϕ), radial (r) and axial (z) co-ordinates, which is described as [74]:

$$r_w = r_o + r_1 \sin(\bar{k}z + m\phi), \tag{2.16}$$

where, r_0 and r_1 is the mean radius and corrugation depth, m is the fold number, and $\bar{k} = 2\pi / d$, d is the SWS period, as shown in Figure 2.7. The SWS reduces the phase velocity of RF generated approximately equals to the beam velocity. The SWS can have mean diameter (D) to free space wavelength ratio, *i.e.*, $D/\lambda_r \approx 1$ for conventional SWS, while $D/\lambda_r \geq 1.5$ for an overmoded SWS. The corrugation depth is such that as,

$$\lambda_r / 16 \leq r_1 \leq \lambda_r / 8 \tag{2.17}$$

The period of SWS is calculated by equating the phase velocity of RF (v_{ph}) to the beam velocity (v_b) and is calculated by

$$v_{ph} \approx v_b, \tag{2.18}$$

where,

$$v_{ph} = \frac{2\pi f_r}{k_z}, \text{ and } v_b \approx c\sqrt{1 - \frac{1}{\gamma_b^2}} \tag{2.19}$$

where, γ_b is the relativistic factor under the influence of space charge effect [74], k_z is π/d for π-mode of operation, which will be explained in detail later, thus substituting this value to (2.18) and (2.19), we get,

$$2df_r \approx v_b, \tag{2.20}$$

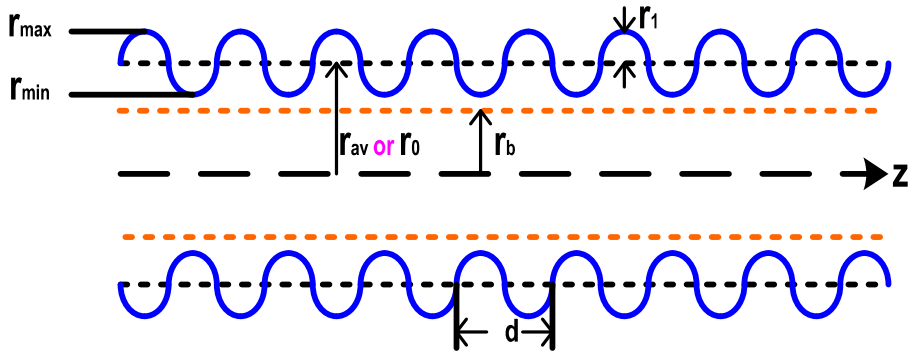

Figure 2.7: 2D Schematic of sinusoidal rippled wall SWS. of the sinusoidally corrugated.

2.3.4 Tapered Waveguide Collector

The decelerated electron beam and unused electrons must be absorbed at the tapered collector, as shown in Figure 2.8, after the interaction through RF within SWS, so that these electrons do not affect the generated RF power and also in order to prevent the damage by the electron beam. The guiding magnetic field is reduced exponentially after the SWS to let the electron beam dumped at the collector. There is a chance that these electrons may damage the collector surface by heating and lets the ions and other molecules to desorb from the surface, which cause the formation of plasma. Now, this plasma can suppress the generated RF power by means of absorbing energy from RF. So, the collector waveguide should be designed carefully for the efficient operation of the device. The simple way is to taper the collector surface such that the incident angle of electron beams gets reduced and the material should have high melting point as well. The up taper angle can vary 4^0 to 6^0 and the length of the up taper is ~$2\lambda r$ [124].

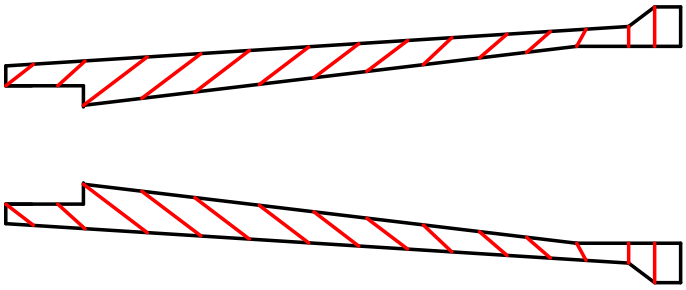

Figure 2.8: 2D Schematic of a tapered collector.

2.3.5 Guiding Magnetic Field

The strong external guiding magnetic field is required to guide the electron beam in the axial direction. In an RBWO, there exists a cyclotron resonance magnetic field at which the suppression of RF power takes place. At this guiding magnetic field value, the electrons gain radial momentum and a part of the EM energy spent on electron rotation, this causes mismatch in Cherenkov synchronism and this affects the generation of RF wave. There are two types of cyclotron resonance absorption generally

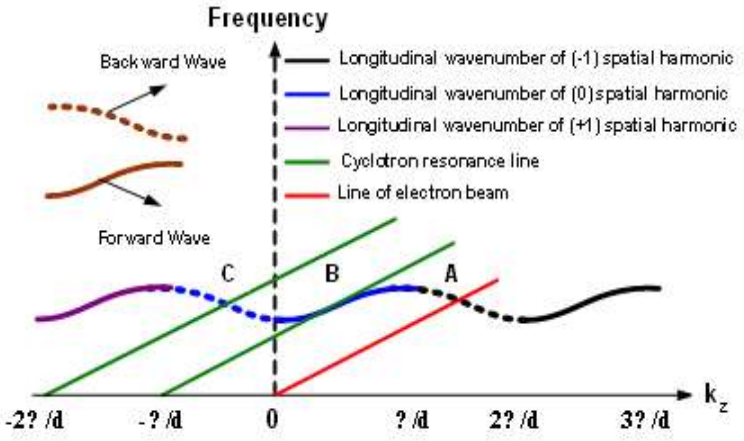

Figure 2.9: A schematic picture of a dispersion relation of TM_{01} mode in infinitely long periodic structure. Two straight lines that intersect the cold structure dispersion curve correspond to Cerenkov and cyclotron beam modes.

occurs in slow-wave devices due to an undesired cyclotron synchronism at the corresponding resonance magnetic field, as shown in Figure 2.9. The first cyclotron synchronism occurs between fundamental space harmonic of the forward wave (*i.e.*, n =

0^{th}) and cyclotron mode of the electron beam and another one is between the fundamental space harmonic of backward wave (*i.e.*, $n = -1^{st}$) and cyclotron mode of the electron beam, respectively. The corresponding resonance magnetic field, B_1 and B_2 related to the cyclotron resonance are described as [125],

$$B_1 = \frac{2mc\gamma_0 v_z}{ed}\left(\frac{\pi}{d} - k_z\right) \tag{2.21}$$

$$B_2 \approx \frac{2\pi mc\gamma_0 v_z}{ed} \tag{2.22}$$

where, γ_0 is the relativistic factor of electron, v_z is the longitudinal velocity of electron, k_z is the longitudinal wavenumber of the fundamental spatial harmonic, d is the period of SWS, c is the speed of light in a vacuum, e and m are the charge and mass of the electron, respectively. Thus, the guiding magnetic field (B) is chosen in between B_1 and B_2 or above B_2.

2.4 Analytical Background of Relativistic BWO

An experimentally tested RBWO device by Kitsanov *et al.* [7] has been considered to develop and validate the analytical modeling for the present studies. The structural and electrical parameters considered are given in Table 2.1**Error! Reference source not found.**. In the experiment, an overmoded SWS ($D/\lambda \approx 1.5$) was considered to overcome the problem of pulse shortening.

2.4.1 Beam Power of thin annular electron beam

Assume a thin electron beam with radius r_b, propagating inside an oversized SWS with radius r_w and guided by a strong external magnetic field such that it's rotational velocity vanishes and beam electron motion restricted to axial direction only. Law of

conservation of energy is applied to calculate the maximum electron beam power such that the sum of both potential and kinetic energies of electrons should be equal to the kinetic energy of the injected electrons [2, 3],

$$(\gamma_b - 1)m_o c^2 + eV = (\gamma_0 - 1)m_o c^2 = eV_0 \tag{2.23}$$

where, γ_b is the actual relativistic factor under the influence of space charge effect and is less than γ_0 due to the voltage depression effect, V is electrostatic potential and e is an electron charge. The solution of electrostatic potential for thin annular beam inside a conducting cylinder is given as [126],

$$V(r_b) = -2\frac{I_b}{v_b}\ln\left(\frac{r_w}{r_b}\right), \quad v_b = c\sqrt{1-\frac{1}{\gamma_b^2}} \tag{2.24}$$

where v_b is axial beam velocity. Finally, the expression for beam current can be written as

$$I_b = \frac{m_o c^2}{e}\frac{1}{2\ln\left(\frac{r_w}{r_b}\right)} v_b\left(\gamma_0 - \gamma_b\right) \tag{2.25}$$

$$= I_A \frac{1}{2\ln\left(\frac{r_w}{r_b}\right)}\left(\gamma_b^2 - 1\right)^{1/2}\left(\frac{\gamma_0}{\gamma_b} - 1\right) \tag{2.26}$$

where, $I_A = 4\pi\varepsilon_o m_o c^3 / e \approx 17.1kA$. The plot of I_b vs γ_b for V_0 = 550 kV and different values of r_b and r_0 is shown in Figure 2.10. It has been observed that $I_b=0$ at γ_b =1 and γ_b = γ_0. The operating region should be selected for γ_b near to γ_0 i.e., $\gamma_0^{1/3} < \gamma_b < \gamma_0$ to minimize the voltage depression due to space charge effect. In between, a maximum value of current will occur when $\gamma_b = \gamma_o^{1/3}$ given as,

$$I_{scl} = \frac{I_A}{2\ln\left(\frac{r_w}{r_b}\right)}\left(\gamma_o^{2/3} - 1\right)^{3/2} \tag{2.27}$$

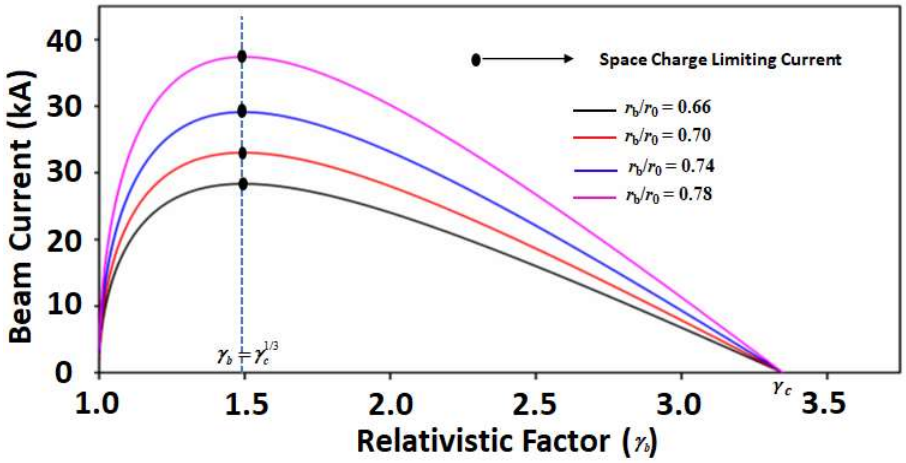

Figure 2.10: The dependence of beam current on γ_b.

The term I_{scl} is the maximum current that the waveguide can allow, and it's called space charge limiting current. The electron beam power can be calculated by the value of beam current and beam voltage as,

$$P_b = I_b V_b = I_b \frac{m_o c^2}{e}\left(\gamma_b - 1\right) \tag{2.28}$$

Substituting (2.24) in (2.26) we get

$$P_b = \frac{I_A}{2\ln\left(\frac{r_w}{r_b}\right)} \gamma_o^2 F\left(\frac{\gamma_b}{\gamma_o}, \gamma_o\right) V_0 \tag{2.29}$$

where V_0 is diode voltage and

$$F\left(\frac{\gamma_b}{\gamma_o}, \gamma_o\right) = \left(\frac{\gamma_b}{\gamma_o} - \frac{1}{\gamma_o}\right)^{3/2} \left(\frac{\gamma_b}{\gamma_o} + \frac{1}{\gamma_o}\right)^{1/2} \left(\frac{\gamma_o}{\gamma_b} - 1\right). \tag{2.30}$$

Next, to find the maximum value of electron beam power it is necessary to find maximum values of $F(\gamma_b/\gamma_o,\gamma_o)$ for each γ_0 and hence a function $W(\gamma_0)$ is introduced and given by:

$$W(\gamma_0)=\max[F(\gamma_b/\gamma_o,\gamma_o)] \tag{2.31}$$

The (2.29) can be rewritten as

$$P_{b,\max}=\frac{I_A V_o}{2\ln\left(\frac{r_w}{r_b}\right)}\gamma_o^2 W(\gamma_0)[GW] \tag{2.32}$$

2.4.2 Dispersion Relation Sinusoidally Corrugated SWS

The wall radius of the sinusoidally corrugated cylindrical waveguide depends on the radial (r) and axial (z) directions with azimuthal symmetry (ϕ = 0), described as:

$$r_w(z)=r_0+r_1\sin(\bar{k}z) \tag{2.33}$$

The schematic representation of the beam within SWS is shown in Figure 2.7. Azimuthally symmetric transverse magnetic (TM) inside cylindrically corrugated waveguide is considered because its axial electric field E_z perturbs the axial velocity of electron beam and low ohmic losses. Due to spatial periodicity of the structure along the axial coordinate z, the axial electric field can be expanded in series according to Floquet's theorem as [74],

$$E_z=\sum_{n=-\infty}^{\infty}E_{zn}(r)\exp\left[i(\omega t-k_n z)\right], \tag{2.34}$$

Where $k_n=k_z+n\bar{k}$ and $-\bar{k}/2\le k_z\le\bar{k}/2$. The different component of EM field intensities E_{zn}, E_{rn}, *and* $H_{\phi n}$ are obtained by considering Maxwell equations and can be written as

$$\frac{1}{r}\frac{d}{dr}\left(r\frac{dE_{zn}}{dr}\right)+k_{\perp n}^2E_{zn}=0,\qquad r\neq r_b, \tag{2.35}$$

where $k_{\perp n}^2=k^2-k_n^2=(\omega/c)^2-k_n^2$. The solution of (2.33) can be given as

$$E_{zn}=\begin{cases}A_nJ_0\left(k_{\perp n}r\right), & 0\le r\le r_b\\ B_nJ_0\left(k_{\perp n}r\right)+C_nY_0\left(k_{\perp n}r\right), & r_b\le r\le r_b\end{cases} \tag{2.36}$$

$$E_{rn}=j\frac{k_n}{k_{\perp n}^2}\frac{dE_{zn}}{dr}, \tag{2.37}$$

$$H_{\phi n}=j\frac{\omega\varepsilon}{k_{\perp n}^2}\frac{dE_{zn}}{dr}, \tag{2.38}$$

where, A_n, B_n and C_n are constants, r_b is beam radius. The constants can be calculated by applying the boundary conditions that at $r = r_b$, the E_{zn} is used to express the coefficients B_n and C_n in terms of A_n as,

$$B_n=A_n\left[1-bJ_0\left(k_{\perp n}r_b\right)Y_0\left(k_{\perp n}r_b\right)\right] \tag{2.39}$$

$$C_n=A_nb\left[J_0\left(k_{\perp n}r_b\right)\right]^2;b=\frac{\omega^2-c^2k_n^2}{\left(\omega-k_nv_b\right)^2}I \tag{2.40}$$

Where $I=c\pi I_b/I_Av_b\gamma_b^3$. Apply the boundary condition, that the tangential component of the electric field at r_w vanishes, thus the condition implies that

$$\left(i\frac{k_n}{k_{\perp n}^2}\frac{dE_{zn}}{dr}\frac{dr_w}{dr}+E_z\right)_{r=r_w}=0, \tag{2.41}$$

substituting (2.32-2.35) in (2.40) and expanding the resulting expression in a Fourier integral over [0, 2π], we find an infinite sum of algebraic equations for the amplitude P_n as

$$\sum_{n=-\infty}^{\infty} P_n D_{mn}\left(\omega, k_z\right) = 0 \tag{2.42}$$

where,

$$D_{mn}\left(\omega, k_z\right) = \left(\frac{\omega^2 - k_m k_n c^2}{k_{\perp n}^2 c^2}\right)\left(I_{mn}^J - \alpha\left(\frac{k_{\perp n} c}{\omega - k_n v_b}\right)^2 \times J_0\left(k_{\perp n} r_b\right)\left[I_{mn}^J Y_0\left(k_{\perp n} r_b\right) - I_{mn}^Y J_0\left(k_{\perp n} r_b\right)\right]\right) \tag{2.43}$$

here α is the space charge factor, given by

$$\alpha = \frac{\pi I_b}{\beta_o \gamma_o^3 I_A} \tag{2.44}$$

where, n is Floquet's space harmonics and m is Fourier space harmonics, $\beta_o = v_z / c = \sqrt{1 - 1/\gamma_b^2}$ is normalized beam velocity and the terms I_{mn}^J and I_{mn}^Y are the integrals of the Bessel functions and polynomials. The non-trivial solution for the dispersion relation obtained by equating the determinant of the homogeneous equation (2.41) to zero, thus,

$$\det\left[D_{mn}\left(\omega, k_z\right)\right] = 0 \tag{2.45}$$

The RF wave is generated in an RBWO by the transfer of energy from drifting electrons to the EM modes of SWS. As the electron beam traverses the SWS, the field gets perturbed, modulates, bunched, and then decelerates the electrons, and this will occur when dispersion curve of a waveguide mode (2.44), intersects with the dispersion curve of the electron beam. For getting a high-quality factor of an interaction circuit, the beam mode line should intersect near about the upper edge of waveguide mode line, *i.e.* ~π point [116], [127]. The dispersion equation for the beam mode line is given by,

$$\omega = k_n v_z , \tag{2.46}$$

The cold dispersion (for α = 0) for an S-band sinusoidally corrugated cylindrical waveguide and dependence of space charge factor on beam current is shown in Figure 2.11. The beam mode line corresponds to 1.2 MV intersects the waveguide mode line having a negative slope [Figure 2.11], which shows that the wave generated has a negative group velocity, *i.e.*, growing in backward direction.

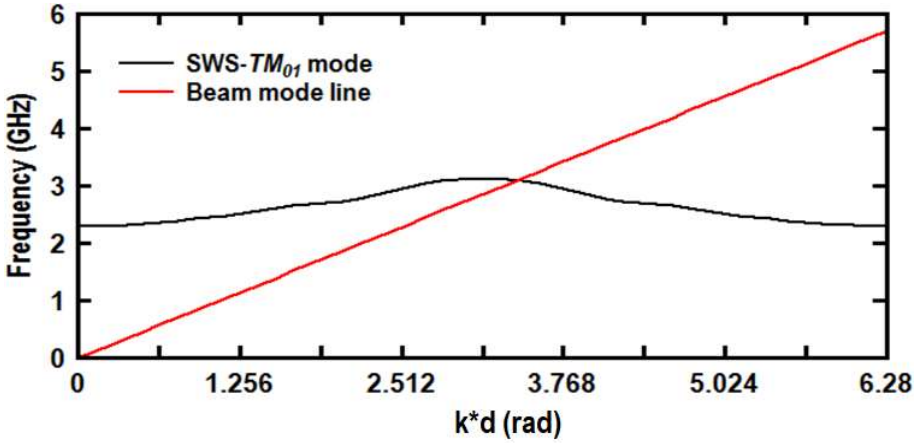

Figure 2.11: The dispersion curve of the beam mode line (1.2 MV) with the TM_{01} mode line.

2.5 Simulation Results and Discussion

An experimental version of S-band overmoded RBWO [7] is examined and validated analytically and also by MAGIC-PIC simulations. The linear and non-linear theories followed by analytical background and modeling of different sub-assembly for an RBWO developed by various researchers, are discussed in this chapter 2.2, and 2.3. The analytical validation of different parameters like beam radius (r_b), cavity RR radius (r_c) and length (L_c), drift section length (L_{dr}) and radius (r_{dr}), SWS radii and period (r_0, r_1, and d), and collector taper angle and length are presented in Section 2.4 of the present Chapter. The beam radius is decided based on cyclotron mode selection theory that gives $r_b \approx 0.7r_0$ for an overmoded SWS to avoid the cyclotron absorption of the

fundamental operating TM_{01} mode. The radii and lengths of RR and drift section is decided analytically based on mathematical relations such that the TM_{02} mode gets locked inside the reflector and the backward propagating TM_{01} mode is reflected back to forward propagating TM_{01} mode. Further, the radii and axial period of SWS are calculated by keeping the mean diameter ~1.5 times the operating wavelength i.e. $D/\lambda \approx 1.5$. The radii are decided such that SWS allow the growth of operating mode and suppress other modes at the operating frequency, while the period is calculated in a manner that it provides the synchronism between the beam axial velocity and phase velocity of RF wave generated. At last, the tapered waveguide collector is designed to collect the used and unused electrons effectively to avoid the localized heating of conductor up to some extent to minimize the generation of collector plasma. The taper angle is decided in between 4^0 to 6^0 and length is around twice of operating wavelength. The parameters have calculated analytically and listed in Table 2.1.

Table 2.1: Design Parameters of an S-band RBWO [7]

	Parameter	**Symbol**	**Values**
Slow-Wave Structure	Mean radius	r_o	62.50 mm
	Corrugation amplitude	r_l	06.00 mm
	Period	d	36.00 mm
	SWS length	N*d	252.00 mm
Reflector	Radius	R_c	79.50 mm
	Length	L_c	40.00 mm
Drift Section	Drift length	L_{dr}	63.80 mm
	Drift Radius	R_{dr}	58.00 mm
Electrical Parameters, Magnetic Field, and Operating Frequency	Beam Radius	r_b	~0.7 r_b
	DC Voltage	V_b	1.2 MV
	Developed Beam Current	I_b	~13.50 kA
	Guiding Magnetic Field	B	2.0 T
	Operating Frequency	f_r	~3.6 GHz

The calculated parameters for cavity RR and TRR are validated by the cold simulation using CST Microwave Studio and after that a complete structure is made in MAGIC-3D to perform and study beam-wave interaction and various parametric analyses to check the sensitivity of the device.

2.5.1 Cold Simulation

The TRR is designed to specify the volume generated by a stencil rotation around the symmetry axis with the VOLUME ROTATE command. With the development of TRR, the absolute electric field in the reflector region is decreased from ~200 kV/cm in RR [Figure 2.12(a)] to ~120 kV/cm [Figure 2.12(b)]. This reduces the radial momentum

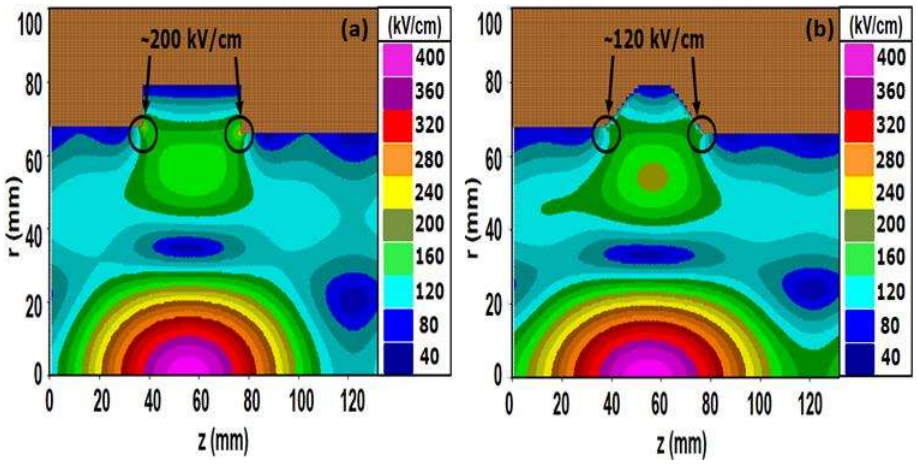

Figure 2.12: Absolute electric field distribution in contour of a cold test, (a) RR and (b) TRR.

spread and improves the bunching by enhancing the electron beam pre-modulation, which in turn increases the RF output power [8, 96] The radius of both TRR and RR are the same, and the length of TRR is adjusted to resonant frequency by slanting the sidewalls of the RR, as shown in Figure 2.12(b).

2.5.2 Particle-In-Cell (PIC) Simulation

The RBWO output RF power enhanced with TRR and overmoded SWS. The optimized parameters of Figure 2.13 are given in Table 2.1. The RF output power is calculated as ~5.4 GW, which is the average power calculated at the end port area of the device with OBSERVE FIELD_POWER S. DA FILTER STEP command, as shown in Figure 2.14 (blue color), with a conversion efficiency of ~33 %. The RF output power of the overmoded RBWO with RR limited to ~5 GW, which is also shown in Figure 2.14 (red color) with a conversion efficiency of ~32 %. The developed beam

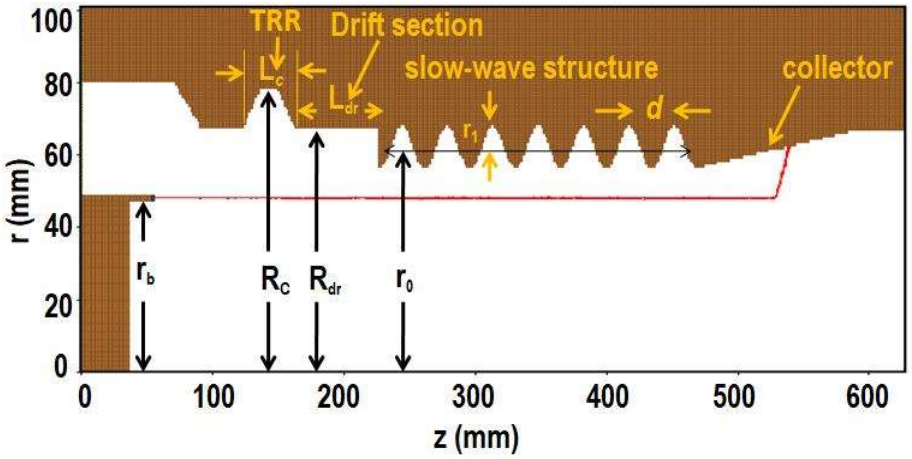

Figure 2.13: The simulation model of RBWO having an electron beam.

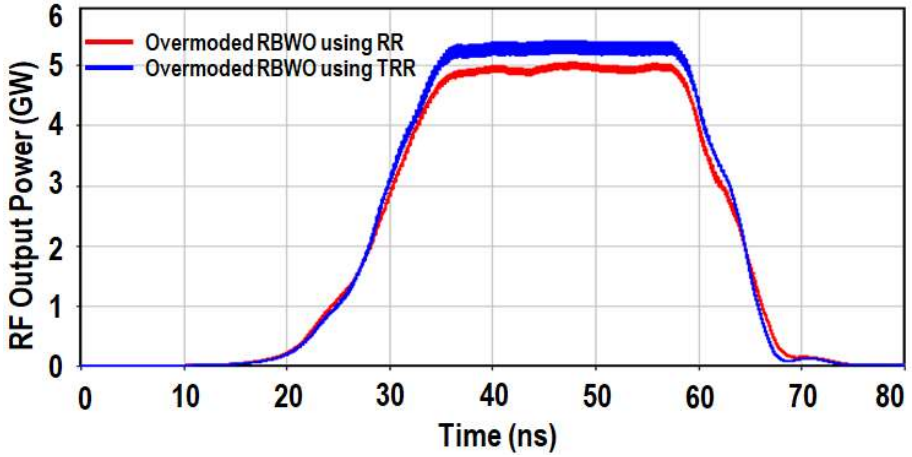

Figure 2.14: RF output powers for the Overmoded RBWO with different reflectors.

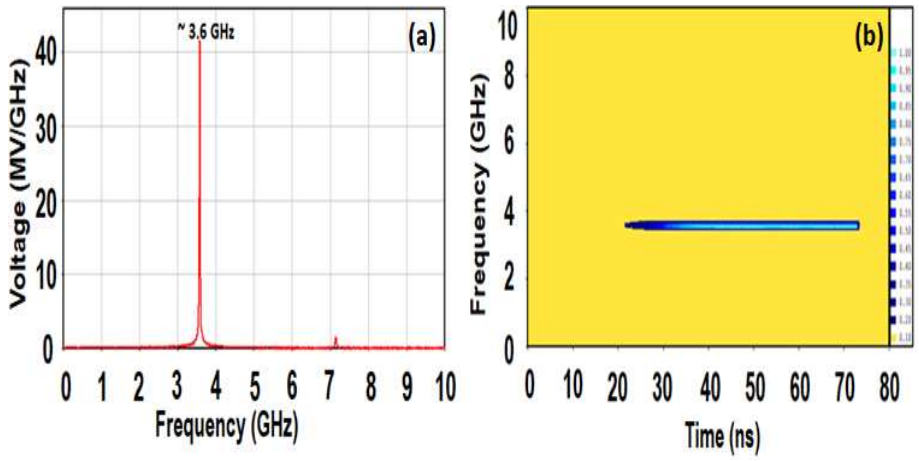

Figure 2.15: (a) Frequency spectrum and (b) The time-frequency of the electric field.

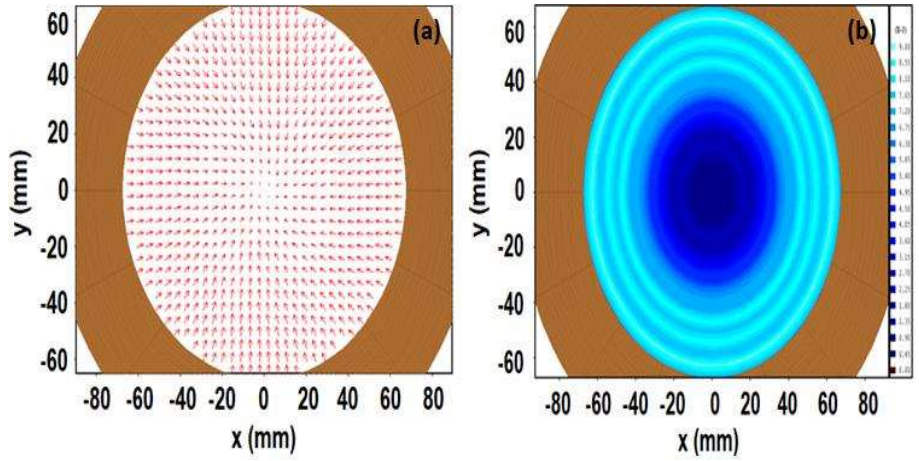

Figure 2.16: Fundamental TM_{01} mode electric field distribution of (a) vector and (b) contour plot.

current ~13.5 kA is measured with 1.2 MV of input DC pulse. An external magnetic field 2.0 T is applied for confining the beam. The obtained RF output power curve is smooth without any disturbance after the saturation. The frequency spectrum [Figure 2.15 (a)] of the corresponding radiated power is calculated by the command OBSERVE FIELD_INTEGRAL E.DL at the end of the device and applying the Fast Fourier Transform (FFT) with a frequency window 0 to 10 GHz. The frequency-time plot for the obtained RF output power is observed in Figure 2.15 (b). The frequency spectrum and frequency-time plots indicate no mode competition, and no harmonics are generated for the device total simulation. Figure 2.16 shows the generated output mode with both vector and contour plot at 55 ns, which is a pure fundamental TM_{01} mode. Other

unwanted modes are eliminated by adequately designing the corrugation amplitude of the SWS [83]. The performance of the proposed device was compared with the earlier works as listed in Table 2.2.

Table 2.2: Comparison of proposed work with previous works.

Parameters	**Ref [117]**	**Ref [7]**	**Proposed work**
Structural Parameters			
Reflector	Cut-off neck	RR	TRR
Electrical Parameters			
Beam Voltage	1.2 MV	1.2 MV	1.2 MV
Developed Beam Current	~15 kA	~15 kA	~13.50 kA
Output Parameters			
Operating Frequency	3.6 GHz	3.6 GHz	~3.6 GHz
Output RF Power	~5 GW	4±1 GW	~5.4 GW
Efficiency	~30.00%	~32.00%	~33.00%

2.6 Parametric Analysis and Discussion

The sensitivity of the device with different design specifications consists of beam voltage, corrugation amplitude, drift length, and the magnetic field is studied.

2.6.1 Beam Voltage (V_b)

As the beam voltage increases, both output RF power and efficiency increase. The increase in beam voltage gives more RF output power, but the efficiency decreases shown in Figure 2.17 (a). The reduction in efficiency of the device is due to the shift in beam mode line towards the left and right from the operating ~π point with the increase and decrease in voltage, respectively. The change in π-point is because of a change in beam velocity with the beam voltage ($\omega = k_z v_b$) that causes the degradation of beam-wave synchronism interaction. The direct effect of reduction in efficiency due to an increase in the developed beam current, as observed in Figure 2.18.

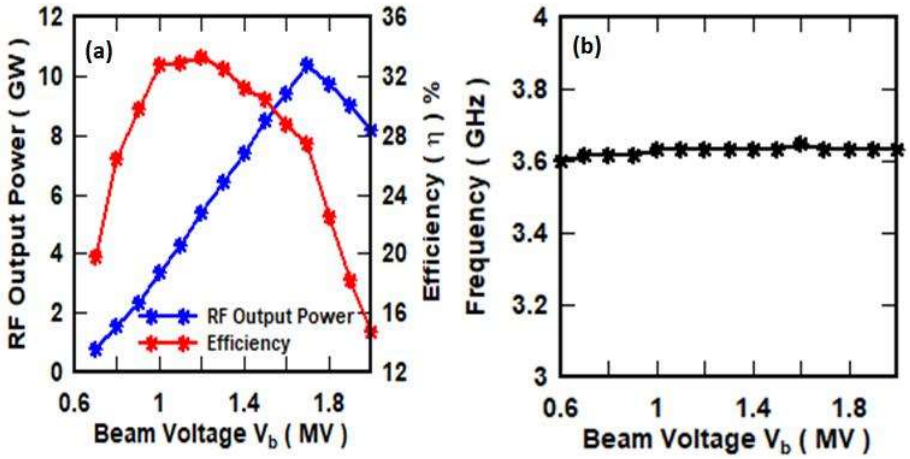

Figure 2.17: Beam voltage depends on (a) RF output power and efficiency and (b) frequency.

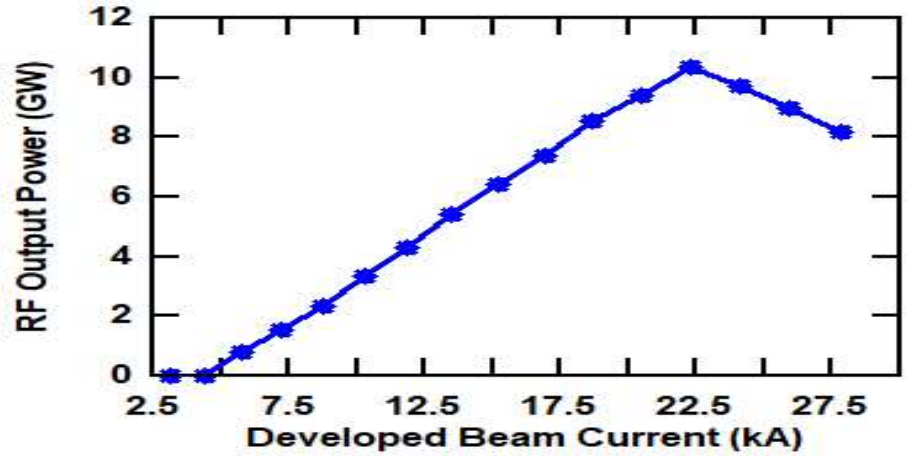

Figure 2.18: Influence of developed beam current on RF output power.

Figure 2.17 (b) shows the variation of the frequency w.r.t the beam voltage. for the beam voltage between 0.6 MV and 2.0 MV, the operating frequency is almost constant. The operating voltage is optimized to 1.2 MV for an RF output power of ~5.4 GW with an efficiency of ~33 % at ~3.6 GHz.

2.6.2 Corrugation Amplitude (r_0)

The operating TM_{01} mode frequency decreases as the corrugation amplitude increases for different SWS period (d) varied from 35 mm to 37 mm, as shown in Figure 2.189 (a). The decrease in frequency improves the separation of TM_{01} from the subsequent next higher mode, i.e., TM_{02}. This results in higher RF output power in the desired

operating TM_{01} mode for the value of r1 from 5 mm to 6 mm [Figure 2.189 (b)]. Further, the increase in corrugation amplitude more than 6 mm reduces the frequency. It decreases the RF output power because in the beam-wave synchronism interruption as the generated frequency also affected with r_1 [Figure 2.19 (a)]. The beam-wave interaction also gets non-synchronized due to the shift in π -point, as the period of SWS is varied. The optimized RF output power [Figure 2.19 (b)] generated for r_1 = 6 mm and d = 36 mm.

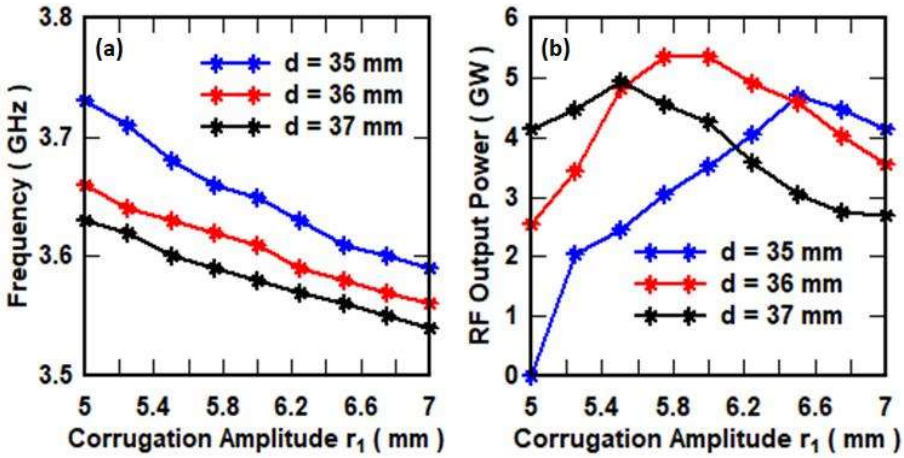

Figure 2.19: Influence of corrugation amplitude on (a) frequency and (b) RF output power with different periods.

2.6.3 Drift Length (L_{dr})

The frequency and RF output power for different drift lengths are shown in Figure 2.20.

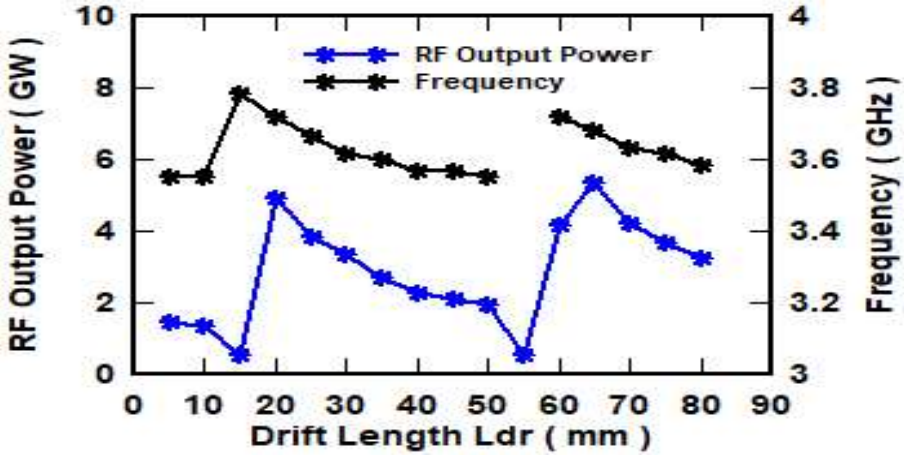

Figure 2.20: RF output power and frequency w.r.t drift length.

Two spikes on the RF output power (blue color) are observed due to phase synchronization of the beam and -1st space harmonic of TM_{01} mode for the various optimal drift lengths (Ldr) [117]. It is observed that the maximum phase synchronization is occurred for Ldr = 63.8 mm. A maximum tuning of ~8 % [Figure 2.20] is achieved around the center frequency between 5 mm and 80 mm of the drift length.

2.6.4 Magnetic Field (*B*)

To achieve a maximum RF output power, the operating magnetic field is optimized by using the PIC simulation of the device [Figure 2.21]. The cyclotron synchronism occurred at B_1 and B_2, which are occurred between the cyclotron mode line and forward wave fundamental space harmonics and the cyclotron mode line and backward wave fundamental space harmonic, respectively. The cyclotron absorption of RF output power is observed at $B_1 \approx 0.12$ T and B_2 ranging from 0.7 T to 0.9 T and these values are well-matched with calculated values by [125] equations (2.21) and (2.22), respectively. The two unwanted cyclotron synchronism resulted in the suppression of output RF power, as observed in Figure 2.21. The maximum and saturated output RF power is obtained at 2.0 T.

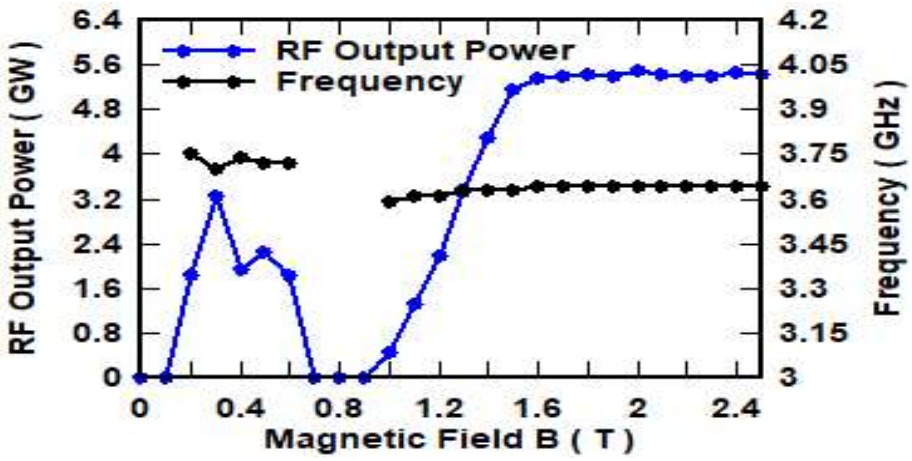

Figure 2.21: **RF output power and frequency w.r.t magnetic field.**

2.7 Conclusion

In this chapter, the operating principle and numerical analysis with design methodology of an RBWO has been discussed. The operating principle along with the fundamental concept for sustained oscillation has presented to understand RF generation in RBWO. Then design methodology for each sub-assembly of an RBWO such as radius of an annular cathode, reflector, drift section, SWS and tapered waveguide collector has been discussed in detail. Later the analytical background of an RBWO was revisited and validated by considering an experimental version of S-band RBWO.

The PIC simulation of RBWO was compared with the experimentally tested RBWO and which is in good agreement with results presented in [7]. In addition to the validation of experimental data, the PIC simulation investigations of an S-band Overmoded RBWO with TRR has been performed by using an FDTD based 3D EM code and found that the use of TRR has reduced the absolute electric field upstream of RBWO, hence improved the power output and the conversion efficiency. The present simulation has predicted an efficiency of ~33 % for an RF output power of ~5.4 GW at ~3.6 GHz. The beam voltage 1.2 MV applied, and ~13.50 kA beam current was developed. Further, the parametric studies were performed to check the device susceptibility with the variation of beam voltage, corrugation amplitude, drift length, and magnetic field.

Further, with this background studies of S-band RBWO few causes of RF pulse shortening have also been identified and investigated under the low guiding magnetic field, as follows in Chapter 3.